Journal of Materials Science: Materials in Electronics (2018) 29:11920–11929
https://doi.org/10.1007/s10854-018-9293-8

Microstructural evolution of Cu–Sn–Ni compounds in full intermetallic micro-joint and in situ micro-bending test

Liping Mo[1] · Chaowei Guo[2] · Zheng Zhou[1] · Fengshun Wu[1] · Changqing Liu[3]

Received: 9 October 2017 / Accepted: 12 May 2018 / Published online: 22 May 2018

Abstract
This study focuses on the microstructural evolution process of Cu–Sn–Ni intermetallic compounds (IMCs) interlayer in the micro-joints, formed from the initial Ni/Sn (1.5 μm)/Cu structure through transient liquid phase (TLP) soldering. Under the bonding temperature of 240 °C, the micro-joints evolve into Ni/(Cu, Ni)$_6$Sn$_5$/(Cu, Ni)$_3$Sn/Cu structure, where the interfacial reactions on Cu/Sn and Sn/Ni are suppressed by the atoms diffusing from the opposite side. The thickness of (Cu, Ni)$_3$Sn layer on plated Cu layer still increases with the prolonged dwell time. When the bonding temperature was elevated to 290 °C, the phase transformation of (Cu, Ni)$_6$Sn$_5$ into (Cu, Ni)$_3$Sn has been accelerated, thus the majority of IMCs interlayer is constituted with (Cu, Ni)$_3$Sn. However, a small amount of Ni-rich (Cu, Ni)$_6$Sn$_5$ phases still remain near the Ni substrate and some of them close to the center-line of IMCs interlayer. The state between (Cu, Ni)$_6$Sn$_5$ and the adjacent (Cu, Ni)$_3$Sn tends to reach equilibrium in Ni content based on the observation from Transmission Electron Microscope (TEM). In addition, the Cu–Sn–Ni IMCs micro-cantilevers were fabricated from these micro-joints using Focus Ion Beam (FIB) for the in situ micro-bending test, the results indicate a high ultimate tensile strength as well as the brittle fracture in the inter- and trans-granular modes.

1 Introduction

The Ni-based under bump metallization (UBM) has been widely used as a barrier to protect the Cu pad from the excessive reaction with Sn-based solder in the conventional flip-chip assemblies [1, 2], and which would be more significant to the miniaturized and multi-functional electronics where the solder bumps have become much smaller than before in the flip chip bonding as well as the 3D IC integration with Cu-pillar bumps [3, 4]. Therefore, numerous studies have been conducted to understand the interfacial reactions in Ni/Sn-based solder/Cu structure. In the microstructural aspect, Cu_3Sn and (Cu, Ni)$_6$Sn$_5$ were observed near the Cu-side, while two layers as a thin layer of (Ni, Cu)$_3$Sn$_4$ with low content of Cu (5 at.%) underneath the (Cu, Ni)$_6$Sn$_5$ were formed on the Ni-side [5–7]. And also, the growth of Cu_3Sn on Cu-side has been suppressed in the Ni/Sn/Cu joints [8]. In particular, the addition of Ni has brought a significant effect on the formation and properties of Cu_6Sn_5 [9, 10]. It can prevent the transformation from the high temperature phase (η-Cu_6Sn_5) to room temperature phase (η′-Cu_6Sn_5) [11] with the minimum requirement of Ni atom only 1 at.% [12]. As a result, the coefficient of thermal expansion (CTE) of (Cu, Ni)$_6$Sn$_5$ is smaller than Cu_6Sn_5 [13], and location of crack initiated in (Cu, Ni)$_6$Sn$_5$ IMC is also different with Cu_6Sn_5 in the joints [14].

However, with the reduced volume of Sn-based solder, the complete consumption of solder would occur instead of the over-corrosion of Cu pads to form intermetallic compounds (IMCs) accompanying with Kirkendall voids [15–17]. Since some phenomena appearing in the micro-joints composed of Cu–Sn–Ni IMCs fully would be different with those joints containing residual Sn-solder, a systematic

✉ Fengshun Wu
fengshunwu@hust.edu.cn

✉ Changqing Liu
C.Liu@lboro.ac.uk

[1] State Key Laboratory of Material Processing and Die & Mould Technology, Huazhong University of Science and Technology, Wuhan 430074, China

[2] Center for Advancing Materials Performance from the Nanoscale (CAMP-Nano) and Hysitron Applied Research Center in China (HARCC), State Key Laboratory for Mechanical Behavior of Materials, Xi'an Jiaotong University, Xi'an 710049, China

[3] Wolfson School of Mechanical, Electrical and Manufacturing Engineering, Loughborough University, Loughborough LE11 3TU, UK

study herein is reported on these Cu–Sn–Ni IMCs micro-joints. On basis of the full IMCs micro-joints preparation, the microstructural evolution within the specific Cu–Sn–Ni IMCs interlayer has been observed and discussed. Moreover, an in situ micro-mechanical testing was also conducted on the Cu–Sn–Ni IMCs layer, as such the maximum fractural stress has been calculated.

2 Materials and methods

2.1 Preparation of Cu/IMCs/Ni structure and microstructural analysis

In this study, commercial Ni substrate with high purity of 99.99 wt% was selected as substrate, on which, a thin Sn layer followed by a Cu layer were sequentially electroplated. Then the initial specimens with Ni/Sn/Cu sandwich structure shown as Fig. 1a were prepared. In order to form the Cu–Sn–Ni IMCs micro-joints effectively, the thin Sn layer (~ 1.5 μm) acts as solder to enable the transient liquid phase (TLP) soldering process [18]. As depicted in Fig. 1b, the specimens were heated up in reflow oven with a ramp up rate of 50°C/min and stayed 2 min at 200 °C to allow them uniformly heated. Afterwards, the specimens were heated up to the bonding temperature (T_B, 240 and 290 °C) with the same heating ratio. In order to achieve fully IMCs micro-joints with different microstructure, the specimens were kept at bonding temperature with different dwell time and cooled down in a mixture of ice water immediately.

The cross-sections of these Ni/IMCs/Cu micro-joints were grinded and polished well, then examined by Field Emission Gun Scanning Electron Microscope (FEG-SEM, Carl Zeiss (Leo)-1530VP) with Energy Dispersive X-ray (EDX) to determine the constituent of IMCs interlayers. Herein, the ratio between each element can be calculated according to the formula (1).

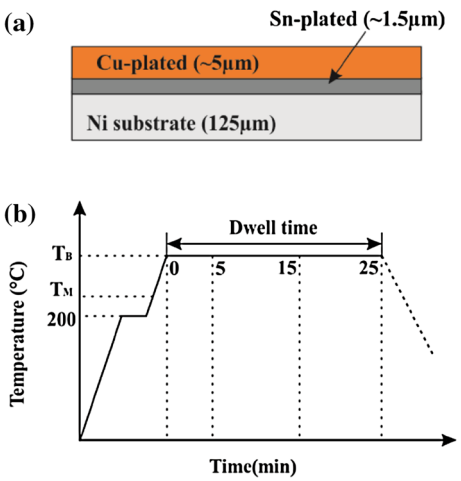

Fig. 1 Schematic diagrams: **a** Ni/Sn/Cu sandwich structure prepared by electroplating; **b** the TLP bonding profile for preparation of the IMCs micro-joints ($T_B > T_M$, T_M: melting temperature of solder)

$$N_{Cu}:N_{Sn}:N_{Ni} = \frac{I_{Cu}}{M_{Cu}}:\frac{I_{Sn}}{M_{Sn}}:\frac{I_{Ni}}{M_{Ni}} \quad (1)$$

where the *Nx, Mx* and *Ix* represent the number of atoms, the molar mass and the intensity of EDX detection about the element of *x* (Cu, Sn or Ni) respectively. Then, a reference line was defined as the ratio of Cu and Sn atoms near the Cu-plated layer reaching the value of 6/5 for the first time, which means the Cu_6Sn_5 IMC formed without the consideration of Ni atoms. The entire IMCs interlayer is thus divided into different layers and their thicknesses can be estimated.

Transmission Electron Microscope (TEM, TECNAI F20, FEI) with higher magnification and resolution was also applied to analyze the change of IMCs interlayer in chemical composition and microstructure, where the specimens were prepared using Focused Ion Beam (FIB, FEI-Nova 600 Nanolab Dual Beam). Finally, through polishing away the top Cu-plated layer, IMCs interlayer of samples was fully uncovered. Then, the types of IMCs phases were confirmed by X-ray diffraction (XRD, XRD-7000s, Shimadzu, Japan).

2.2 Fabrication of micro-cantilevers and in situ bending testing

The micro-cantilevers at the selected IMCs regions were fabricated by FIB with its micro-milling function. The size of these micro-cantilevers is approximately 1 μm × 1 μm × 5 μm, which was guaranteed by the processing sequence as ①, ②, ③ in Fig. 2a, b with the current of 7 nA or 2.8 nA to remove the bulk, and 93 pA to refine the surfaces. The micro-bending test was conducted by the nano-mechanical test system (Hysitron PI 87 SEM PicoIndenter) in FIB chamber. The indenter was loaded from the front of these IMCs micro-cantilevers with the velocity of 10 and 20 nm/s respectively, as demonstrated in Fig. 2c. The deformation behavior of micro-cantilevers in the testing process was monitored and recorded simultaneously.

3 Results and discussion

3.1 Growth kinetics of $(Cu, Ni)_3Sn$ in Cu–Sn–Ni IMCs micro-joints

The cross-sectional morphologies of Cu–Sn–Ni IMCs micro-joints forming at 240 °C with different dwell time (0/5/15/25 min) are shown in Fig. 3. Two sub-layers can be seen in the IMCs interlayer, and some voids appeared

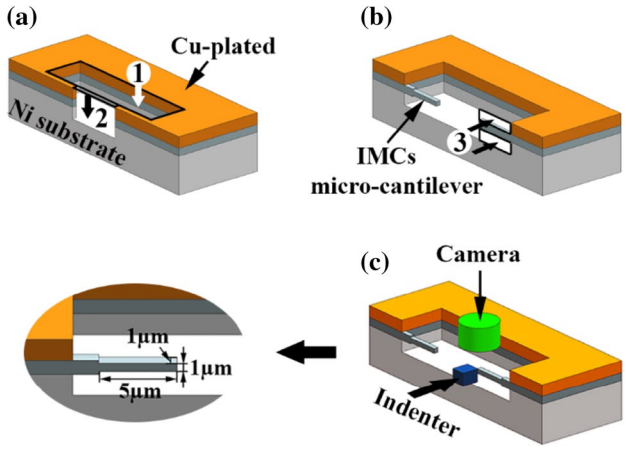

Fig. 2 Schematic diagrams: **a, b** fabrication sequence of IMCs micro-cantilevers by FIB (① remove the bulk of material to make sure cantilevers with certain width, ② remove the material between two cantilevers to define the length of them, ③ remove the material around IMCs interlayer to get the cantilevers with certain height); and **c** the in situ mechanical testing

around the interface between Cu-plated layer and IMCs when the dwell time is 25 min. According to the EDX results in Table 1, the dark grey area on the Cu side is $(Cu, Ni)_3Sn$, and the other light grey area near Ni side is $(Cu, Ni)_6Sn_5$ where the content of Ni increased slightly with the dwell time. Besides, the Ni–Sn IMCs (Ni_3Sn_4 or Ni_3Sn_2) layer, which can be produced from the reactions between Ni and Sn, is hardly to be recognized in these IMCs micro-joints. This can be attributed to the suppressing effect by lots of Cu atoms diffusing from Cu-plated layer to Ni substrate [6], or the Ni–Sn IMCs layer is too thin to be distinguished by the FEG-SEM.

According to the EDX line-scanning result in Fig. 3, the lines mark the Cu_6Sn_5 phase boundary out from others when $I_{Sn} \approx 15{,}000$, $I_{Cu} \approx 10{,}000$, the N_{Cu}/N_{Sn} ratio is about 1.2. Therefore, the IMCs interlayer can be divided into three regions: the Cu-rich layer as $(Cu, Ni)_3Sn$ IMC adjacent to the Cu-plated substrate; the Sn-rich layer as Cu_6Sn_5 IMC with high Sn content in the middle area; and the thin Ni-rich layer on the Ni substrate. The thickness of each individual IMCs layers is measured and given in Fig. 4 (the variation was produced by the measuring error). From this figure, the thickness of Cu-rich layer increases while the thickness of Sn-rich layer decreases with the dwell time. But the change of Ni-rich layer is insignificant. The growth of Cu-rich layer in the micro-joints with short dwell time (less than 5 min) is resulted from the interfacial reactions, such as Sn+(Cu, Ni) → $(Cu, Ni)_3Sn$ on the Cu-plated layer/IMCs interface, and Cu+$(Cu, Ni)_6Sn_5$ → $(Cu, Ni)_3Sn$ on Cu-rich layer/Sn-rich

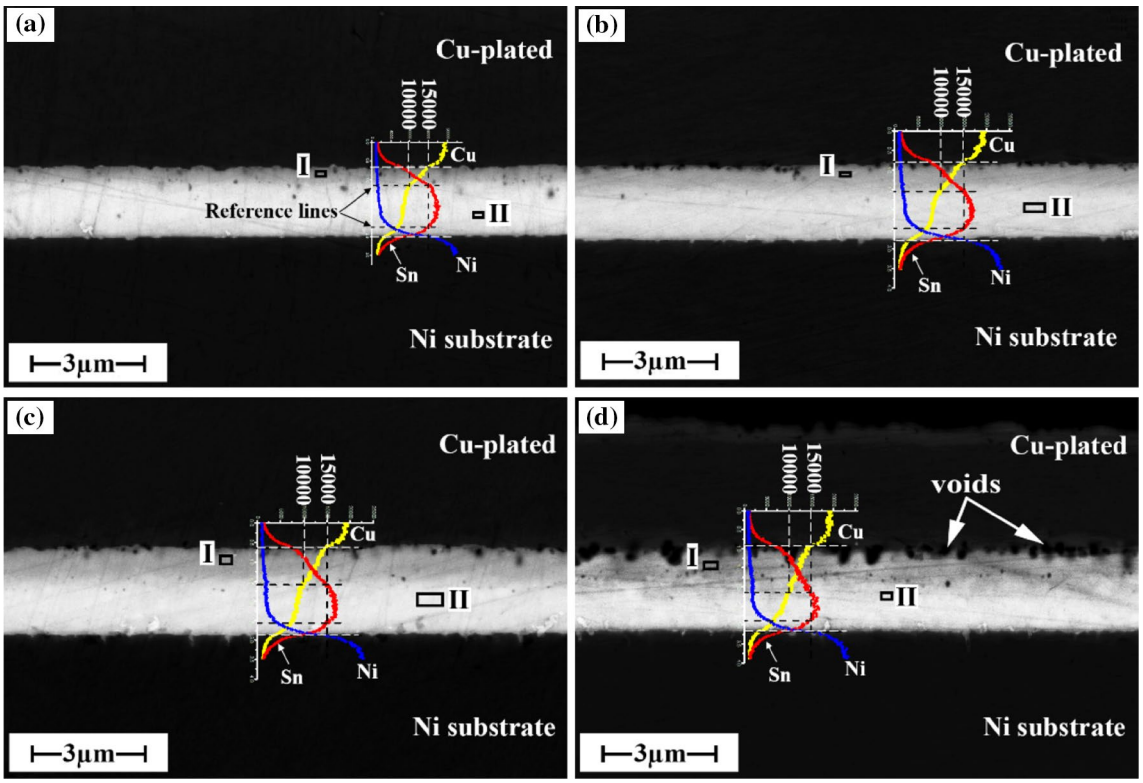

Fig. 3 SEM images and EDX line-scanning results on the cross-section of IMCs micro-joints formed under 240 °C with different dwell time **a** 0 min; **b** 5 min; **c** 15 min; **d** 25 min

Table 1 EDX results from FEG-SEM observation on IMCs interlayer formed at 240°C

Dwell time	0 min		5 min		15 min		25 min	
Atomic percent (at.%)	I	II	I	II	I	II	I	II
Cu	77.0	52.4	71.3	50.0	73.1	52.7	72.0	55.1
Sn	20.6	42.7	25.8	42.2	24.4	40.3	24.8	36.3
Ni	2.5	4.9	2.9	7.7	2.5	7.0	3.2	8.5

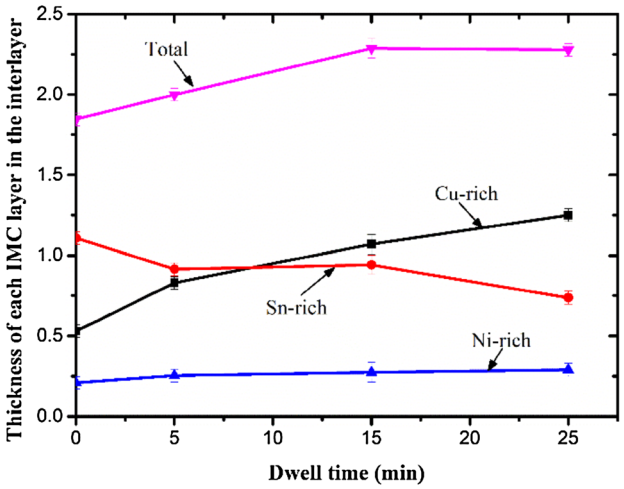

Fig. 4 Thickness of each layer in IMCs interlayer formed under 240 °C with different dwell time

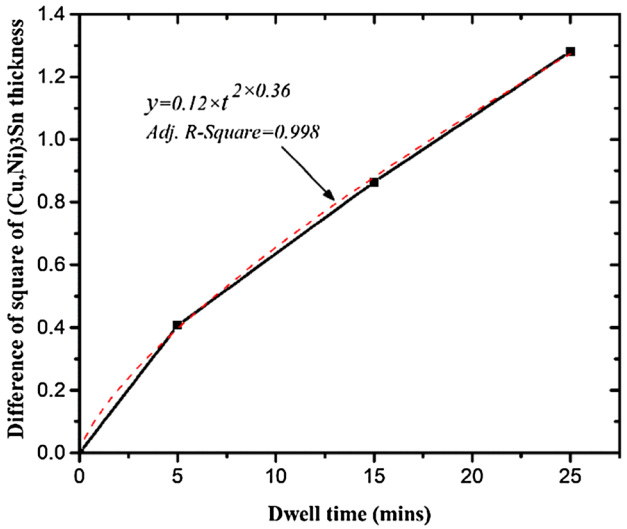

Fig. 5 Interfacial growth kinetics of (Cu, $Ni)_3Sn$ fitted by empirical formula

layer. Because of the dominant reaction at the Cu-plated layer side, the total thickness of IMCs interlayer has been increased. When the dwell time is in the range of 5–15 min, the growth of Cu-rich layer slows down, for the thick Cu-rich layer has delayed the diffusing time of Cu and Sn atoms to the reaction interfaces. After that, the total thickness of IMCs interlayer is kept stable, and the Cu-rich layer has become thicker with the depletion of Sn-rich layer as the main route. Meanwhile, the emerging micro-voids have also retarded the reaction on the Cu-plated layer/IMCs interface to some extent.

Furthermore, the empirical formula (2) [19] is used to characterize the growth behavior of (Cu, $Ni)_3Sn$ with the prolonged dwell time at 240 °C in this Cu/IMCs/Ni structure.

$$y = d_t^2 - d_0^2 = K \times t^{2n} \quad (2)$$

where d_0 and d_t are the (Cu, $Ni)_3Sn$ thickness at the beginning and after a certain dwell time (t), respectively; K is the coefficient and n refers to the growth factor of (Cu, $Ni)_3Sn$. The fitting result plotted in Fig. 5 yields a growth factor (n) 0.36, which is smaller than the value of Cu_3Sn growing in the Cu/Sn/Cu structure (0.48) under the same soldering condition [20]. This indicates the participation of Ni atoms in micro-joints has accelerated Sn atoms in the Cu_6Sn_5 layer diffusing to the Ni substrate, as well as stabilized the Cu_6Sn_5 phase to impede the phase transformation of Cu_6Sn_5 into Cu_3Sn [8].

3.2 Microstructural characteristics of Cu–Sn–Ni IMCs micro-joints

The microstructure of Cu–Sn–Ni IMCs micro-joints formed at higher bonding temperature (290 °C) is shown in Fig. 6. The cross-section morphology of micro-joint with the dwell time of 0 min (Fig. 6a) is similar with the ones formed at 240 °C. However, the layer-structure of IMCs interlayer cannot be observed clearly in the micro-joint of 5 min dwell time. The composition on different areas of these IMCs interlayers is provided in Table 2. Comparing with the result in Table 1, the Sn content of the Sn-rich layer has decreased to 33.77 at.% accompanying with the increasing Ni to 15.01 at.% in the micro-joint of 5 min dwell time at 290 °C. Nevertheless, the gradient change of (Cu, $Ni)_3Sn$ layer is negligible for the different bonding temperature and dwell time. When the dwell time is extended to 15 min, the Sn-rich layer has transformed into (Cu, $Ni)_3Sn$ and the whole IMCs interlayer seems to be homogeneous. Especially, a thin and discontinuous greyish substance remains on the Ni substrate with a high Ni content of 22.5 at.% (Fig. 6c-III).

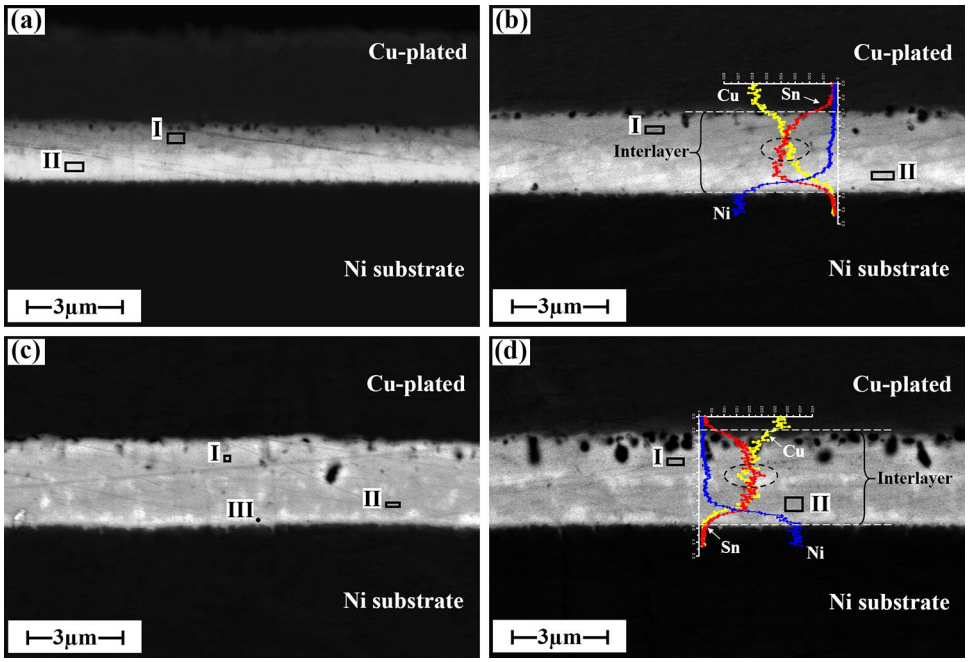

Fig. 6 SEM images and EDX line-scanning results on the cross-section of IMCs micro-joints formed under 290 °C with different dwell time **a** 0 min; **b** 5 min; **c** 15 min; **d** 25 min

Table 2 EDX results from FEG-SEM observation on IMCs interlayer formed at 290°C

Dwell time	0 min		5 min		15 min			25 min	
Atomic percent (at.%)	I	II	I	II	I	II	III	I	II
Cu	75.0	48.2	74.49	51.22	72.6	66.2	48.4	73.39	59.21
Sn	22.4	39.1	22.67	33.77	24.8	27.6	29.1	23.94	25.3
Ni	2.5	12.7	2.84	15.01	2.6	6.2	22.5	2.67	15.49

And some light grey phases distribute around the center-line of IMCs interlayer in the micro-joints with 25 min dwell time (Fig. 6d). Moreover, it is indicated by the line-scanning profiles that these light grey phases also appear in the micro-joint with a shorter dwell time (e.g. 5 min), where a sudden rise occurs in the content of Sn and Ni along with the decrease of Cu content, highlighted by elliptical dashed-lines in Fig. 6.

More details have been revealed by TEM observation on the micro-joint formed with a dwell time of 25 min at 290 °C in Fig. 7. The IMCs interlayer is constituted with fine grains, the sizes of which are less than 1 μm. The constituent of IMCs interlayer has been inspected thoroughly, given in Table 3. It is clear that with a lower magnification and resolution, the EDX results from FEG-SEM have a relative higher Ni content from a larger area of analysis, in comparison with the results from TEM, but still reasonable to reflect the distribution of elements in IMCs interlayer. Moreover, the Ni segregation occurs in the middle of IMCs interlayer as illustrated in the elemental mapping images, the composition of which is similar with the Ni-rich layer on Ni substrate. And the Ni content in surrounding $(Cu, Ni)_3Sn$ is only in the range of 1–5 at.%, which falls within the region of Ni content between $(Cu, Ni)_6Sn_5$ and $(Cu, Ni)_3Sn$ in the equilibrium solidification of Cu–Sn–Ni alloy revealed by the other researchers [21].

3.3 Discussion on microstructural evolution

In order to better identify the types of Cu–Sn–Ni IMCs in these micro-joints, XRD analysis has been applied on the IMCs interlayers from three representative micro-joints: (1) soldered at 240 °C for 15 min, having the typical two-layer structure of IMCs interlayer; (2) soldered at 290 °C for 5 min, where the interfaces between different IMC layers become undistinguishable; and (3) formed after a long dwelling of 25 min at 290 °C, in such case the Ni segregation appears in the IMCs interlayer. The XRD results as presented in Fig. 8 are evident that the main components of IMCs interlayer in these micro-joints under the soldering temperature of 240–290 °C are $(Cu, Ni)_6Sn_5$ and $(Cu, Ni)_3Sn$, which is consistent with the results of EDX analysis. Ni_3Sn_4 IMC was detected only in the micro-joints soldering at 240 °C for 15 min indicating that the Ni–Sn reaction has actually happened between the Ni substrate and Sn solder layer during the soldering process. However, it is too thin to

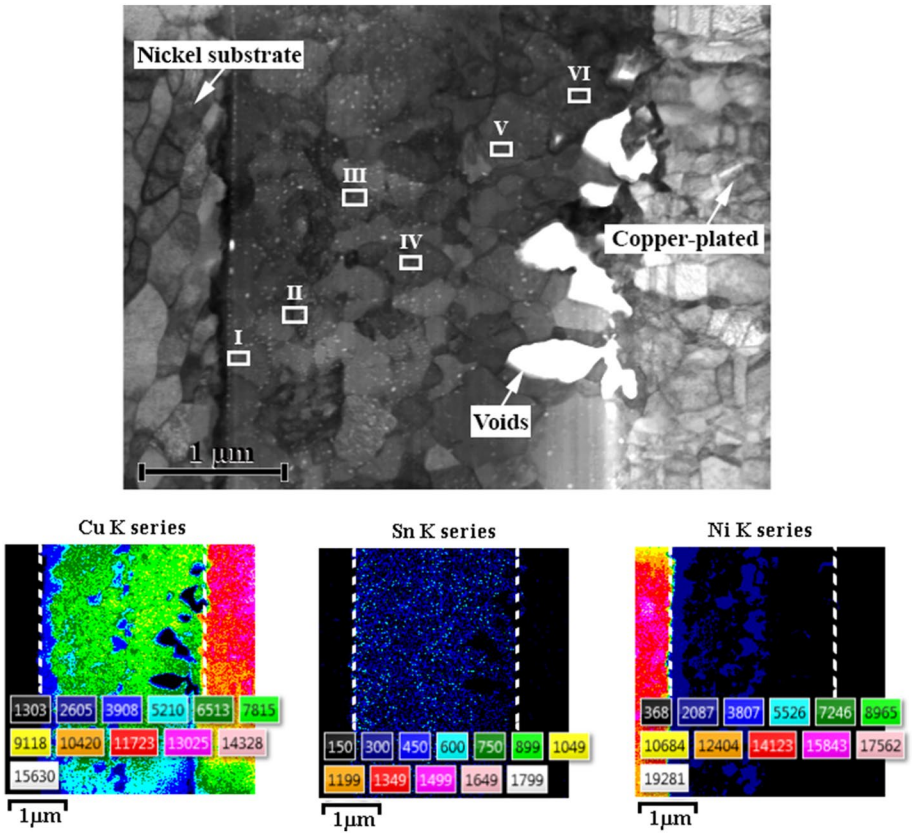

Fig. 7 TEM bright field observation on the IMCs interlayer formed at 290 °C with a dwell time of 25 min (above) and the mapping result (below)

Table 3 EDX results from TEM observation on IMCs interlayer formed at 290 °C with 25 min

Atomic percent (at.%)	I	II	III	IV	V	VI
Cu	39.3	65.9	79.7	46.7	79.3	80.5
Sn	39.9	28.9	18.8	33.3	19.7	19.0
Ni	20.9	5.2	1.5	20.1	1.1	0.5

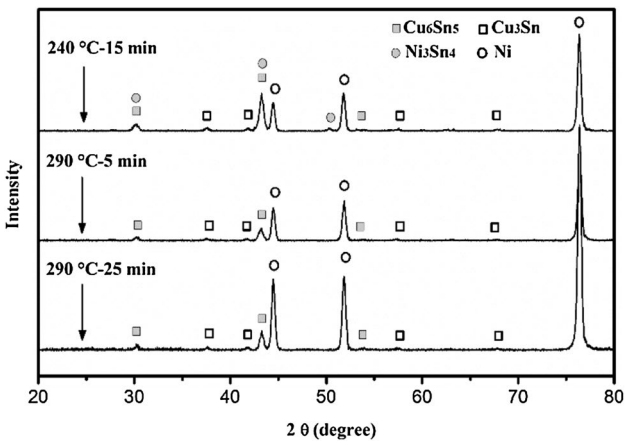

Fig. 8 XRD detection results of the Cu–Sn–Ni IMCs interlayers

be detected through the FEG-SEM observation. In addition, the composition of IMCs interlayer has not changed for the dwell time at 290 °C, and any of the Ni–Sn IMCs products do not appear in the micro-joint even dwelled up to 25 min.

On the basis of Cu–Sn and Ni–Sn binary phase diagrams [22, 23], the reaction types and phase constitution almost remain the same in the temperature range of 240–290 °C. Therefore, the hypothesis can be made and the microstructure of micro-joints formed at 290 °C for certain dwell time will be similar with the micro-joints formed at 240 °C for a relative long dwell time. The experimental data obtained from Cu–Sn–Ni IMCs composition analysis in those micro-joints can be plotted on the Cu–Sn–Ni ternary phase diagram at 240 °C [21] shown in Fig. 9, where the red-triangle points represent the data combining the SEM-EDX and

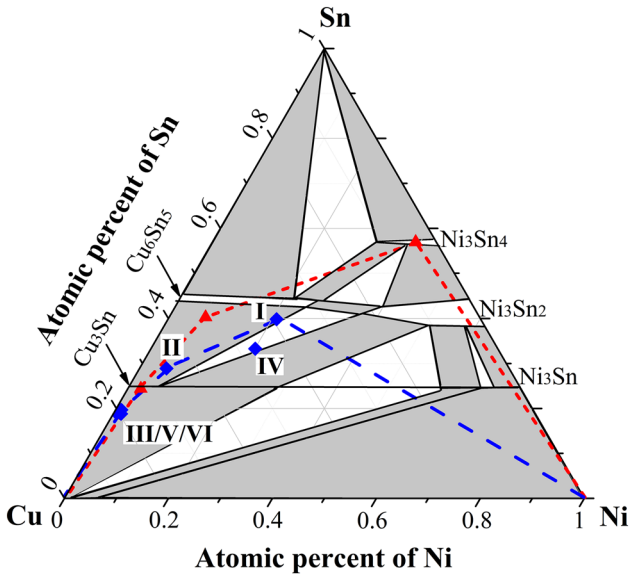

Fig. 9 The evolution path of Cu–Sn–Ni IMCs in micro-joints under 240–290 °C (filled traingle—the results from the micro-joint formed at 240 °C for 15 min; filled diamond—the results from the micro-joint formed at 290 °C for 25 min)

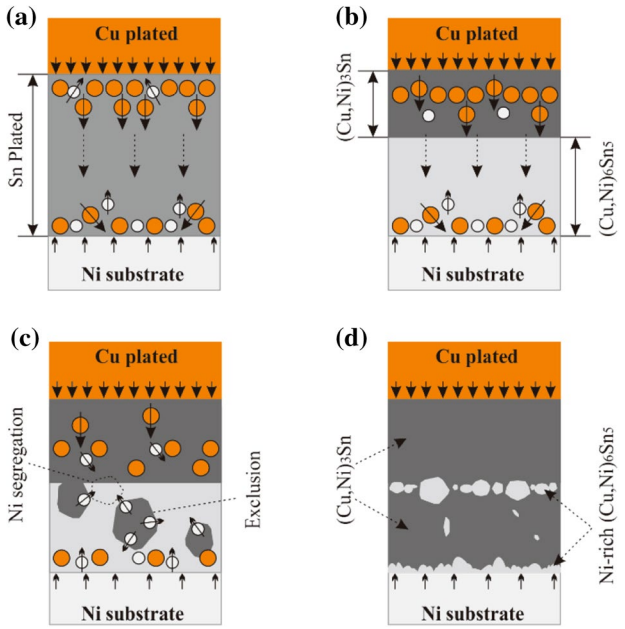

Fig. 10 Microstructural evolution process of Cu–Sn–Ni IMCs micro-joints (filled circle: Cu atom; open circle: Ni atom): **a** Cu and Ni atoms diffusing in the molten Sn layer; **b** IMCs interlayer formed containing (Cu, Ni)$_3$Sn and (Cu, Ni)$_6$Sn$_5$ mainly; **c** (Cu, Ni)$_6$Sn$_5$ transformed into (Cu, Ni)$_3$Sn with the exclusion of Ni atoms and then Ni segregation occurred; **d** Ni-rich (Cu, Ni)$_6$Sn$_5$ appeared near the center-line of (Cu, Ni)$_3$Sn interlayer and Ni substrate

XRD results on micro-joint formed at 240 °C for 15 min, while the blue-diamond points are from the TEM-EDX measurement on micro-joint formed at 290 °C for 25 min. The dashed lines connecting the different points reveal the diffusion paths of Cu and Ni atoms in these solid Cu–Sn–Ni IMCs micro-joints at 240–290 °C, and the indicative range of IMCs composition can be deduced from the diagram. It is evident that Cu atoms diffuse faster than Ni atoms in IMCs interlayer, the increase of Cu atoms content with dwell time makes the microstructure of IMCs interlayer changed dramatically. Also, the inter-reaction has taken place in the Ni/IMCs/Cu structure, since the thin interconnecting height of micro-joints allowed lots of Cu atoms diffusing into the Sn/Ni interface quickly at high bonding temperature. The initial product (Ni_3Sn_4) from Ni–Sn reaction has been evolved from $Ni_3Sn_4 + Cu \rightarrow (Cu, Ni)_6Sn_5$. Otherwise, the Cu–Sn reaction has become predominant on the Ni substrate to suppress the Ni–Sn reaction, thus the (Cu, Ni)$_6$Sn$_5$ has been produced directly for the Cu–Sn–Ni ternary reaction.

Based on the above findings, the microstructural evolution process of these Ni/IMCs/Cu micro-joints can be described by some systematic schematics in Fig. 10, where the yellow dots are described as Cu atoms and the grey dots are Ni atoms. During the TLP soldering process, significant amount of Cu atoms was dissolved into molten Sn and migrated to Ni substrate within a short time. At the same time, few Ni atoms were dissolved into Sn and arrived at the Cu layer due to the lower diffusion rate, as shown in Fig. 10a. The solidification and IMCs formation have formed an initial IMCs micro-joint which consists of Ni/(Cu, Ni)$_6$Sn$_5$/(Cu, Ni)$_3$Sn/Cu, where a very thin layer of Ni_3Sn_4 is negligible as presented in Fig. 10b.

After solidification, the diffusion of Cu and Ni atoms in the solid is the main mechanism for the microstructural evolution of these micro-joints. Through the reaction of (Cu, Ni)$_6$Sn$_5$ + Cu → (Cu, Ni)$_3$Sn, the (Cu, Ni)$_3$Sn layer has thickened in a layered structure. As a result, the thickness of (Cu, Ni)$_6$Sn$_5$ layer has deceased and the Ni content in (Cu, Ni)$_6$Sn$_5$ layer has increased. Because of the emerging of Ni-rich area near the center-line of IMCs interlayer, the interface between two types of IMC layers has become ambiguous for a long-time dwelling. This evolution process can be explained by the suppression of Ni atoms in the (Cu, Ni)$_3$Sn layer by the diffusion of Cu atoms, as such they moved out along with the migration direction of Cu atoms. Therefore, the Ni content around the (Cu, Ni)$_3$Sn/(Cu, Ni)$_6$Sn$_5$ interface is much higher than the other area. Besides, the lower solid solubility of Ni in Cu_3Sn than that in Cu_6Sn_5 makes the redundant Ni atoms to be excluded from the initial (Cu, Ni)$_6$Sn$_5$ grains in the phase transformation process, causing the segregation of Ni atoms. Since the higher content of Ni atoms keeps the (Cu, Ni)$_6$Sn$_5$ grains more stable in thermal dynamics [21], these Ni-rich (Cu, Ni)$_6$Sn$_5$ grains have been thus preserved near the center-line, even though the other (Cu, Ni)$_6$Sn$_5$ grains have transformed into (Cu,

$Ni)_3Sn$, as depicted by Fig. 10c. In addition, because the Ni atoms continued to diffuse from Ni substrate into IMCs interlayer for the existence of chemical concentration gradient, with a relative low diffusion rate, the thin Ni-rich $(Cu, Ni)_6Sn_5$ layer has formed on the Ni substrate. This has led to the final microstructure of Cu–Sn–Ni IMCs micro-joints as illustrated in Fig. 10d.

3.4 In situ micro-bending test on Cu–Sn–Ni IMCs micro-cantilevers

Three groups of Cu–Sn–Ni IMCs micro-cantilevers were fabricated by FIB in the micro-joints forming at 290 °C with 0 min dwelling, as shown in Fig. 11. There are three groups with six micro-cantilevers in total and each micro-cantilever is labelled, for example No. 1-L is the left micro-cantilever in group 1. The micro-bending tests have been carried out through the movement of indenter downward with 10 nm/s, expect the left one in group ③ was loaded with 20 nm/s. Three major sequential stages were observed during the in situ micro-bending test as demonstrated in Fig. 12. Obviously, a small amount of deformation occurred during the indenter loading, and the Cu–Sn–Ni IMCs micro-cantilevers have fractured from the root part when the load has increased to certain level.

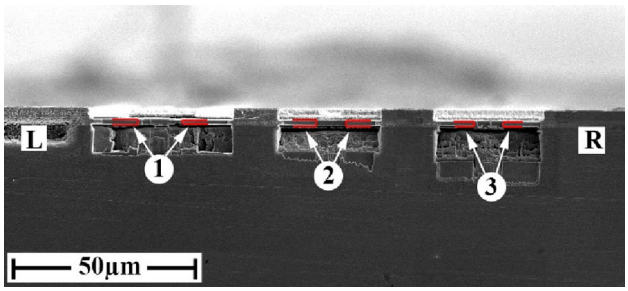

Fig. 11 The front view of three groups of IMCs micro-cantilevers in the micro-joint formed at 290 °C with 0 min (L: left side, R: right side)

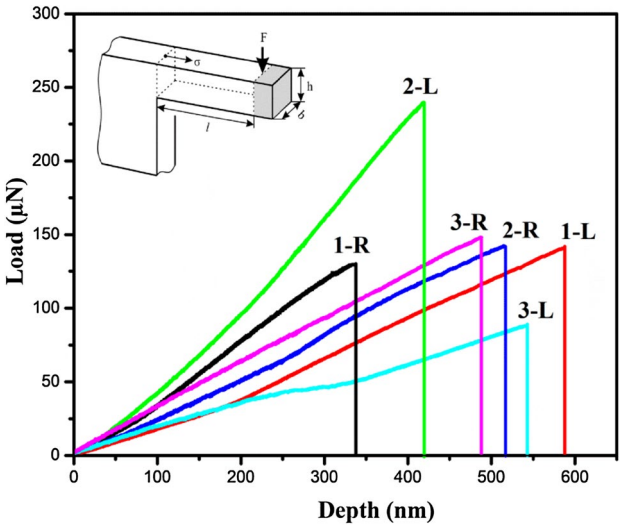

Fig. 13 Load-depth profiles from in situ micro-bending test and the calculation of ultimate tensile strength

The load-depth profiles derived from the in situ micro-bending test are depicted in Fig. 13, and the stress state of these IMCs micro-cantilevers has been analysed through the formula (3).

$$\sigma_{max} = \frac{6 \times F_{max} \times l}{b \times h^2} \tag{3}$$

Because of the intrinsic rigidity and brittleness of IMCs, the tip of micro-cantilever has been treated as rigid object. Herein, the loading force is regarded as a concentrated force (F) on the certain location. Once the fracture occurred, the loading force reached the peak value (F_{max}), then the tensile stress in the horizontal direction (σ) on the root became maximum. Considering the relevant geometrical factors, such as the arm length (l), the width (b) and the height (h) of micro-cantilever, the ultimate tensile stress (σ_{max}) has been calculated and listed in Table 4. The average σ_{max} of this type of Cu–Sn–Ni IMCs is 2.3 ± 0.7 GPa, which is reasonable to compare with the ultimate tensile strength of single crystal

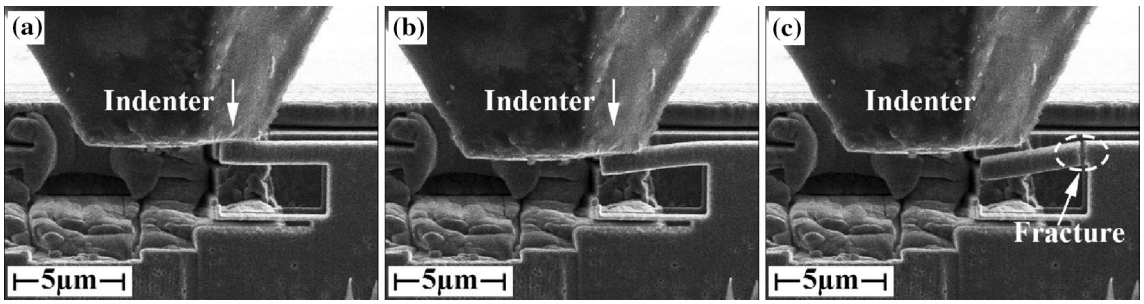

Fig. 12 Three major stages during the in situ micro-bending test observed from the top view of IMCs micro-cantilevers **a** contact; **b** loading and deformation; **c** fracture

Table 4 Parameters of IMCs micro-cantilevers and the calculated σ_{max}

Parameters	1-L	1-R	2-L	2-R	3-L	3-R
l (μm)	3.32	3.41	3.41	3.32	3.41	3.74
h (μm)	1.07	1.18	1.22	1.05	1.02	1.23
b (μm)	1.22	0.67	1.21	1.12	1.01	1.12
F_{max} (μN)	142.32	140.85	129.79	148.20	87.99	239.79
σ_{max} (GPa)	2.0	3.1	1.5	2.4	1.7	3.2
$\overline{\sigma}_{max}$ (GPa)	2.3 ± 0.7					

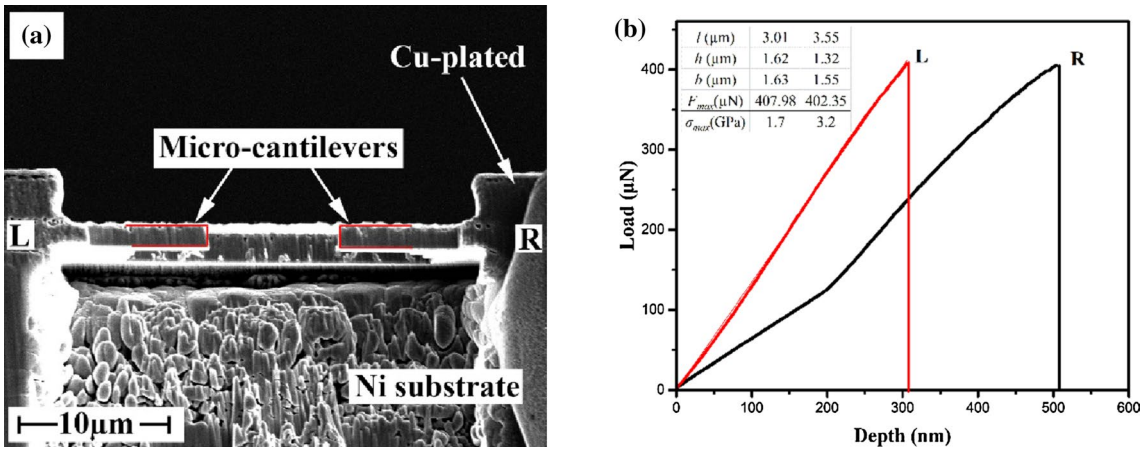

Fig. 14 **a** the front view of IMCs micro-cantilevers in the micro-joint formed at 290 °C with 25 min; **b** the load-depth profiles from the in situ micro-bending test (L: left side, R: right side)

Cu_3Sn calculated in reference [24]. Meanwhile, it is worth of noticing that the deformation behavior of IMCs micro-cantilevers has not been affected by the different loading rate, but the stress values have a big fluctuation due to the inconsistent geometric size of micro-cantilevers.

More tests have been conducted on the IMCs micro-cantilevers in micro-joint formed with a dwell time of 25 min at 290 °C, as shown in Fig. 14. The displacement rate of indenter was set as 20 nm/s. The ultimate tensile strengths obtained from the two IMCs micro-cantilevers are 1.7 and 3.2 GPa, respectively. The large fluctuation between them is suppose to depend on the inhomogeneous microstructure of IMCs beams, however, the values are still in the scale range from the prior tests. The fracture surfaces of these two micro-cantilevers have further observed by SEM at a high magnification (Fig. 15). The morphology is uneven, but including many small cleavage planes. In particular, the intact grain remains inside the center of micro-cantilever (Fig. 15b), which is supposed to be the Ni-rich $(Cu, Ni)_6Sn_5$ grain. All of the observation exhibits that both the transgranular and intergranular fracture have occurred in the Cu–Sn–Ni IMCs micro-cantilevers, however, the deformation behavior and the fracture modes of them are not sensitive with the microstructural change of IMCs interlayer for the prolonged dwell time.

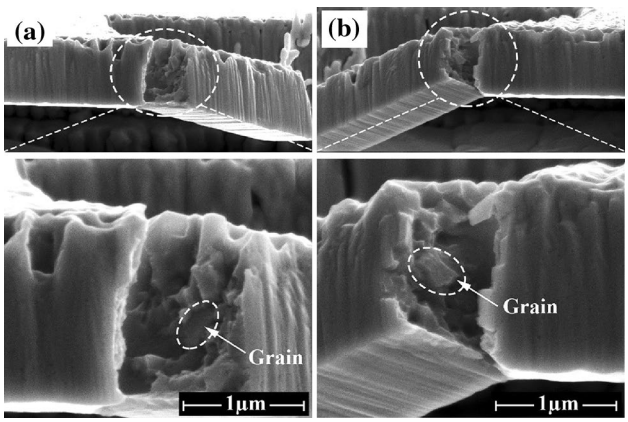

Fig. 15 Enlarged images of fracture morphologies of IMCs micro-cantilevers after testing

4 Conclusions

The microstructure of IMCs interlayer in the Cu/IMCs/Ni micro-joints has been studied during the process of TLP soldering at 240 °C and 290 °C for different dwell time. Under the lower temperature, the growth of layered $(Cu, Ni)_3Sn$ adjacent to Cu layer is the major microstructural

change in the IMCs interlayers with the prolonged dwell time. Because of the thin interconnected height of micro-joints, the phenomenon of inter-reaction has been a main feature in these Ni/IMCs/Cu micro-joints. The growth of (Cu, Ni)$_3$Sn layer turns out to be suppressed by the Ni atoms diffusion, where the growth factor of 0.36 is relatively small compared with the Cu_3Sn layer in the Cu/IMCs/Cu joints. Meanwhile, since a significant amount of Cu atoms have diffused to Ni substrate, the Ni-rich (Cu, Ni)$_6$Sn$_5$ has replaced the Sn-Ni product (Ni_3Sn_4) or generated directly from the Cu–Sn–Ni reaction on the Ni substrate.

The Ni segregation exists near the center-line of Cu–Sn–Ni IMCs interlayers forming at 290 °C with the dwell time longer than 5 min. This is attributed to the exclusion of Ni atoms from (Cu, Ni)$_3$Sn layer driven by the diffusion of Cu atoms and the phase transformation from (Cu, Ni)$_6$Sn$_5$ into (Cu, Ni)$_3$Sn. Therefore, Ni atoms have congregated in some local area where the (Cu, Ni)$_6$Sn$_5$ grains are stabilized. In addition, the results from in situ micro-bending tests show that the ultimate tensile strength of Cu–Sn–Ni IMCs micro-cantilevers is approximately 2.3 GPa, at the point of the inter- and trans-granular fractures, irrespective of the microstructural change of IMCs interlayers with the dwell time at 290 °C.

Acknowledgements This work was supported by the National Nature Science Foundation of China [NSFC No. 61574068] and the Fundamental Research Funds for the Central Universities [No. 2016JCTD112]. The author L Mo would like to acknowledge the support from the joint research degree program between Loughborough University and Huazhong University of Science and Technology. All the authors appreciate the technical help from the Center for Advancing Materials Performance from the Nanoscale (CAMP-Nano) and Hysitron Applied Research Center in China (HARCC) in Xi'an Jiaotong University for the in situ mechanical testing.

References

1. B. Lee, H. Jeon, K.-W. Kwon, H.-J. Lee, Employment of a bi-layer of Ni(P)/Cu as a diffusion barrier in a Cu/Sn/Cu bonding structure for three-dimensional interconnects. Acta Mater. **61**, 6736–6742 (2013)
2. J.G. Duh, Interface reactions and phase equilibrium between Ni/Cu under-bump metallization and eutectic SnPb flip-chip solder bumps. J. Mater. Res. **18**, 935–940 (2003)
3. B. Lee, H. Jeon, S. Kim, K. Kwon, J.-W. Kim, H. Lee, Introduction of an electroless-plated Ni diffusion barrier in Cu/Sn/Cu bonding structures for 3D integration. J. Electrochem. Soc. **159**, H85-H89 (2011)
4. M.-H. Chan, Y.-C. Liao, C.-T. Lin, K.-W. Chuang, H.-N. Huang, C.-T. Yeh, W.-T. Tseng, J.-Y. Lai, Thermal cycling effect on intermetallic formation with various surface finish of micro bump interconnect for 3D package, IEEE 63rd Electronic Components and Technology Conference (ECTC), pp. 2163–2167 (2013)
5. R. Labie, W. Ruythooren, J. Van Humbeeck, Solid state diffusion in Cu–Sn and Ni–Sn diffusion couples with flip-chip scale dimensions. Intermetallics **15**, 396–403 (2007)
6. C. Liu, C. Ho, C. Peng, C.R. Kao, Effects of joining sequence on the interfacial reactions and substrate dissolution behaviors in Ni/Solder/Cu joints. J. Electron. Mater. **40**, 1912–1920 (2011)
7. S.-W. Chen, S.-H. Wu, S.-W. Lee. Interfacial reactions in the Sn-(Cu)/Ni, Sn-(Ni)/Cu, and Sn/(Cu,Ni) systems. J. Electron. Mater. **32**, 1188–1194 (2003)
8. V. Vuorinen, T. Laurila, T. Mattila, E. Heikinheimo, J. Kivilahti, Solid-state reactions between Cu(Ni) alloys and Sn. J. Electron. Mater. **36**, 1355–1362 (2007)
9. J.-W. Yoon, S.-W. Kim, S.-B. Jung, Interfacial reaction and mechanical properties of eutectic Sn–0.7Cu/Ni BGA solder joints during isothermal long-term aging. J. Alloys Compd. **391**, 82–89 (2005)
10. J.-W. Yoon, S.-W. Kim, S.-B. Jung, IMC morphology, interfacial reaction and joint reliability of Pb-free Sn–Ag–Cu solder on electrolytic Ni BGA substrate. J. Alloys Compd. **392**, 247–252 (2005)
11. U. Schwingenschlögl, C. Di Paola, K. Nogita, C.M. Gourlay, The influence of Ni additions on the relative stability of η and η′Cu_6Sn_5. Appl. Phys. Lett. **96**, 061908 (2010)
12. Y.Q. Wu, S.D. McDonald, J. Read, H. Huang, K. Nogita, Determination of the minimum Ni concentration to prevent the η to η4 + 1 polymorphic transformation of stoichiometric Cu_6Sn_5. Scripta Mater. **68**, 595–598 (2013)
13. K. Nogita, D. Mu, S.D. McDonald, J. Read, Y.Q. Wu, Effect of Ni on phase stability and thermal expansion of $Cu_{6-x}Ni_xSn_5$ (x = 0, 0.5, 1, 1.5 and 2). Intermetallics **26**, 78–85 (2012)
14. D. Mu, H. Huang, S.D. McDonald, J. Read, K. Nogita, Investigating the mechanical properties, creep and crack pattern of Cu_6Sn_5 and (Cu, Ni)$_6$Sn$_5$ on diverse crystal planes. Mater. Sci. Eng. A **566**, 126–133 (2013)
15. N. Bosco, F. Zok, Critical interlayer thickness for transient liquid phase bonding in the Cu–Sn system. Acta Mater. **52**, 2965–2972 (2004)
16. B.S. Lee, S.K. Hyun, J.W. Yoon, Cu–Sn and Ni–Sn transient liquid phase bonding for die-attach technology applications in high-temperature power electronics packaging. J. Mater. Sci.: Mater. Electron. **28**, 7827–7833 (2017)
17. F. Gao, J. Qu, Calculating the diffusivity of Cu and Sn in Cu_3Sn intermetallic by molecular dynamics simulations. Mater. Lett. **73**, 92–94 (2012)
18. J.F. Li, P.A. Agyakwa, C.M. Johnson, Interfacial reaction in Cu/Sn/Cu system during the transient liquid phase soldering process. Acta Mater. **59**, 1198–1211 (2011)
19. T.-T. Luu, A. Duan, K. Aasmundtveit, N. Hoivik. Optimized Cu–Sn wafer-level bonding using intermetallic phase characterization. J. Electron. Mater. **42**, 3582–3592 (2013)
20. L. Mo, F. Wu, C. Liu. Growth kinetics of IMCs in Cu–Sn intermetallic joints during isothermal soldering process. 2015 IEEE 65th Electronic Components and Technology Conference (ECTC), pp. 1854–1858 (2015)
21. H. Yu, V. Vuorinen, J.K. Kivilahti, Solder/substrate interfacial reactions in the Sn–Cu–Ni interconnection system. J. Electron. Mater. **36**, 136–146 (2007)
22. S. Fürtauer, D. Li, D. Cupid, H. Flandorfer. The Cu–Sn phase diagram. Part I: new experimental results. Intermetallics **34**, 142–147 (2013)
23. C. Schmetterer, H. Flandorfer, K.W. Richter, U. Saeed, M. Kauffman, P. Roussel, H. Ipser. A new investigation of the system Ni–Sn. Intermetallics **15**, 869–884 (2007)
24. H.-C. Cheng, C.-F. Yu, W.-H. Chen. Strain- and strain-rate-dependent mechanical properties and behaviors of Cu_3Sn compound using molecular dynamics simulation. J. Mater. Sci. **47**, 3103–3114 (2012)